GPS Solutions (2023) 27:89
https://doi.org/10.1007/s10291-023-01421-9

ORIGINAL ARTICLE

Feature-based GNSS positioning error consistency optimization for GNSS/INS integrated system

Xiaoji Niu[1,2,3] · Yuhang Dai[1] · Tianyi Liu[1] · Qijin Chen[1,2] · Quan Zhang[1,3]

Received: 19 April 2022 / Accepted: 15 February 2023

Abstract

The estimated GNSS positioning error, which is commonly represented by measures such as variance or standard deviation, will determine the weight of measurements in the Kalman filter of GNSS/INS integration and significantly affect the integrated navigation results. However, there is a substantial inconsistency between the estimated error provided by GNSS solutions and the actual GNSS positioning error, especially in harsh environments like urban canyons. Previous research has primarily focused on detecting and processing GNSS gross errors to reduce the impact on GNSS/INS integrated systems, while the consistency of the estimated GNSS error has not received much attention. Hence, this work focuses on optimizing GNSS error estimation based on machine learning to improve the consistency with the actual positioning error and the reliability of the GNSS/INS integrated system. An integrated classification and regression tree and bootstrap aggregating (CART-Bagging) algorithm was applied to construct the classification model, and the observation-based features were employed for consistency optimization. Field datasets covering typical urban scenes (e.g., open-sky environment and complex urban environment) over 24 h were collected to assess the accuracy of the GNSS quality control method. The test results showed that the classification accuracy of the estimated GNSS positioning error is more than 90%, and the consistency of GNSS positioning error and the accuracy of integrated positioning are improved by approximately 70% and 30%, respectively.

Keywords GNSS error estimation · Quality control · GNSS/INS · Machine learning · CART-Bagging

Introduction

The global navigation satellite system (GNSS) and inertial navigation system (INS), with autonomous navigation characteristics, display significant complementary advantages (Groves 2013), and the combined system using the Kalman filter fusion algorithm has been widely applied in the high-precision autonomous driving industry (Shin 2005). The GNSS/INS integrated system has been proven to be a reliable and efficient integrated mode while providing continuous and centimeter-level positioning using real-time kinematics (RTK) technology in the open-sky environment (Takasu and Yasuda 2009). However, the accuracy and reliability of GNSS positioning are significantly reduced owing to gross errors (e.g., multipath effect, non-line-of-sight signals) caused by various effects in complex GNSS environments. Moreover, the estimated error of the GNSS positioning solutions does not match the actual positioning accuracy (Niu et al. 2018). This inconsistency significantly influences the measurement weight in Kalman filtering, thereby further affecting the positioning accuracy of the GNSS/INS integrated system.

Numerous studies have been aimed at detecting the gross errors of GNSS positioning in the GNSS/INS integrated navigated system. The traditional GNSS quality control method evaluates positioning quality through features such as elevation (EL), carrier-to-noise density ratio (C/N_0), and the number of satellites (N_{SAT}) (Zhou et al. 2018). It also sets thresholds to improve the overall observation quality and enhance accuracy. However, threshold setting depends on experience and must be tailored for each instance. Niu et al. (2018) augmented the GNSS colored noise as a state vector of an integrated navigation algorithm to improve the consistency of the estimated error. Although the online

✉ Quan Zhang
zhangquan@whu.edu.cn

1 GNSS Research Center of Wuhan University, Wuhan, China

2 Artificial Intelligence Institute of Wuhan University, Wuhan, China

3 Hubei Luojia Laboratory, Wuhan, China

Published online: 19 March 2023

estimation largely resolves the issue of observation noise being non-white to ensure the consistency of final integrated navigation results, this approach cannot achieve the consistency of GNSS positioning results. Alternatively, innovation filtering in the GNSS/INS integrated navigation system (Groves 2013) is commonly used for quality control by weighting observations based on measurement accuracies. Innovation filtering is highly effective at detecting short-term gross errors, such as measurements in a GNSS tracking loop close to loss of lock; however, innovation robustness relies on observation noise and only works well when the state and the measurement covariance matrices can represent their respective actual errors (Meng et al. 2016). In complex urban scenes, the inconsistent estimated error affects the accuracy of innovation filtering. Although current quality control methods mostly guarantee or improve upon the GNSS positioning accuracy, there are few research and analyses on the consistency between the estimated GNSS position error and actual positioning error.

Recent studies have demonstrated that machine learning techniques can be employed to facilitate GNSS positioning. For example, Drawil et al. (2012) trained a model based on the number of satellites (N_{SAT}), dilution of precision (DOP), signal-to-noise ratio (SNR), and the speed of the vehicle reported by the GNSS receiver, dividing the resulting GNSS positioning accuracy into three accuracy bands. To further enhance GNSS positioning accuracy, Hsu (2017) employed a support vector machine (SVM) classifier to distinguish three types of GNSS pseudorange measurements (line-of-sight, multipath, and non-line-of-sight). Sun et al. (2021) used a gradient boosting decision tree (GBDT)-based method to predict the pseudorange errors. In the navigation-to-navigation (Nav2Nav) application, Socharoentum and Karimi (2016) implemented both machine learning algorithms and pseudorange corrections to jointly detect NLOS signals, achieving an average accuracy ratio of 90%. Xu et al. (2020) indicated that machine learning could be used to estimate sky visibility and the boundaries of surrounding buildings to reflect the visibility of satellites better and improve positioning results. By formulating the multipath estimation as a regression problem, Phan et al. (2013) constructed a nonlinear continuous model for estimating multipath error based on support vector regression, thereby improving GNSS positioning accuracy. Although most research aimed at GNSS signal error detection (e.g., NLOS) for improving the actual GNSS positioning accuracy, few studies have investigated the application of machine learning for consistency optimization between estimated GNSS position error and the actual positioning accuracy. The consistency is important in GNSS/INS integrated navigation because it directly affects the reasonable weight allocation of observation information.

Accordingly, this work focuses on optimizing the estimated GNSS position error to improve the consistency with the actual positioning error and promote the reliability of GNSS/INS integrated navigation. A machine learning approach is proposed to detect GNSS positioning outliers and improve the corresponding estimated error. Specifically, a classification model based on the GNSS observation features (e.g., *EL*, C/N_0, and N_{SAT}) was built to precisely classify GNSS positioning accuracy into ten classes. The predicted quality class is then employed to modify the estimated error and improve upon the consistency between the estimated GNSS error and the actual positioning accuracy. Lastly, the optimized GNSS position error estimation was applied to the GNSS/INS integrated navigation solution to verify the reliability of the proposed method. The contributions of this approach can be summarized as follows:

(1) An integrated classification and regression tree and bootstrap aggregating (CART-Bagging) algorithm was proposed to optimize the GNSS error estimation method and improve consistency with actual accuracy;
(2) Observation-based features were divided into four groups and adopted into the proposed classification method without complicated data preparation and processing;
(3) GNSS/INS integrated system was employed to validate the practicality and improvement effect of the proposed consistency optimization of GNSS position errors.

An overview of the proposed method is given in the following section. First, the CART-Bagging algorithm for classifying GNSS position error estimation is described. Then, the CART-Bagging-based GNSS quality control method for better estimation consistency is discussed straightforwardly. Finally, field test results are analyzed to evaluate the proposed consistency optimization method of GNSS position error through classification, GNSS, and integrated navigation aspects, and a comparison with the traditional threshold setting method is also conducted to assess reliability.

Bootstrap aggregating

Machine learning is often used for prediction and analysis, especially for unknown new data, as it builds statistical probability models by experience to improve system performance (Rao 2005). Indeed, the growing abundance of GNSS software receivers and raw data in recent years has laid a foundation for new methods of GNSS data processing based on machine learning (Favenza et al. 2016). Sufficient data and abundant features can be employed to build the optimization method for estimating GNSS positioning error to ensure its consistency with actual accuracy.

The proposed approach applies a fully labeled dataset corresponding to the GNSS positioning accuracy to different

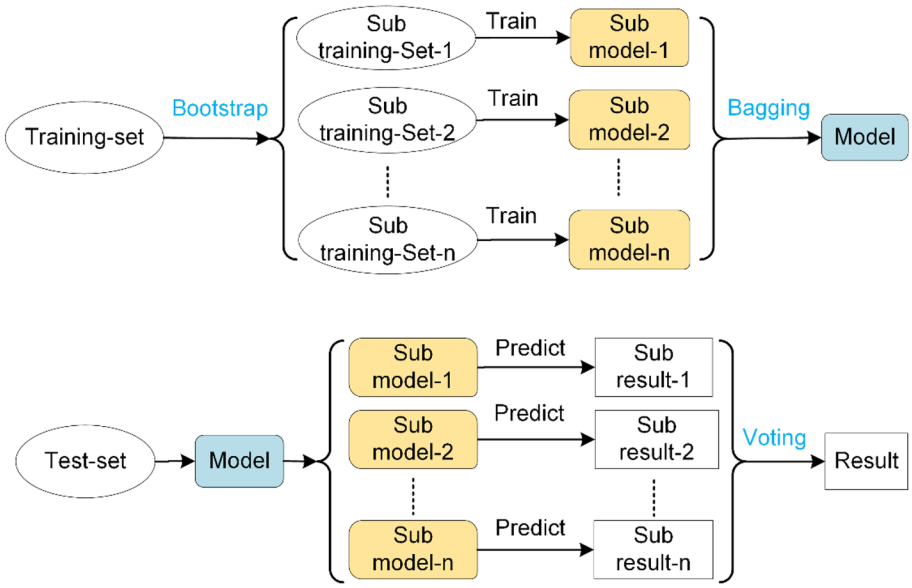

Fig. 1 Flow diagram for the machine learning based on decision tree: Bagging training process (top panel) and Bagging testing process (bottom panel)

classes. It fits the characteristics of a supervised model of machine learning. As a common supervised learning technique, the decision tree determines the topological structure between features through attribute selection (Quinlan 1986). Here, considering the classification and regression tree (CART) algorithm can support pruning with no split limit by applying recursive binary trees, it was employed in the decision tree to output the probability distribution under the given input conditions. The principle of Gini index (Tangirala 2020) minimization was defined for feature selection and building the binary tree model in the CART classification. The *Gini(D)* index chosen here represents model impurity, where the smaller the index value, the more accurate the features:

$$Gini(D) = \sum_{i=1}^{K} p(x_i) * \left(1 - p(x_i)\right) = 1 - \sum_{i=1}^{K} p(x_i)^2 \qquad (1)$$

where K is the number of classes, and $p(x_i)$ represents the probability that the sample point x belongs to class i. Accordingly, the features with the smallest Gini index and the corresponding nodes were selected to generate the CART. To prevent overfitting, the decision tree was pruned by calculating the cost function of each subtree, and the optimal subtree was selected via cross-validation techniques (Sutton 2005).

Figure 1 shows the flow diagram for the machine learning based on the decision tree. Since the generalization ability of a single learner is weak and local optimization is easy to occur, the ensemble multiple decision trees can form a more stable and comprehensive model. Bootstrap aggregating (Bagging) is a common ensemble technique which can improve both the stability and predictive power of classification trees (Breiman 1996), as it constructs multiple independent and uncorrelated base classifiers, each of which is randomly sampled with replacement and performs parallel training across all samples to obtain the base model (top panel in Fig. 1). Because the GNSS gross errors account for a relatively small proportion, the random sampling process of Bagging can increase the probability of detecting anomalies. Therefore, Bagging was deemed more suitable for the present study. Prediction models based on multiple trainings can achieve more accurate classification by voting (bottom panel in Fig. 1).

Considering the advantages of the CART and Bagging algorithms, this work proposes the integrated CART-Bagging classification tree as the consistency optimization method for GNSS positioning error, as shown in Table 1. This method fits the characteristics of GNSS measurements and has high classification accuracy.

Quality control methodologies

GNSS features are analyzed first before describing the traditional threshold setting method and the CART-Bagging-based optimization method for estimating GNSS positioning errors proposed here. Lastly, performance evaluation indicators were listed for assessment.

Features analysis

For the traditional threshold setting method and the consistency optimization method based on CART-Bagging, selecting the GNSS features for analysis represent a formative step. While the traditional method sets thresholds for features based on experience and receiver implementation,

Table 1 CART-Bagging algorithm

Algorithm 1: CART-Bagging

Input:

Number of learners N

Maximum number of splits M

GNSS features $\boldsymbol{x}$

Class Grade of estimated GNSS positioning error y

Training data set $T = \{(\boldsymbol{x_1}, y_1), (\boldsymbol{x_2}, y_2), \cdots, (\boldsymbol{x_k}, y_k)\}$

Initialize:

Learning algorithm $CART$

Function Bagging ($CART$, N, M, T)

For m = 1 to N do

$T_m \leftarrow$ bootstrap sample from the training set T

$$h_m \leftarrow CART(T_m)$$

End for

$$h_f(x) \leftarrow sign\left(\sum_{m=1}^{N} T_m(x)\right)$$

Return $h_f(x)$

Output: the mode of the predicted value of each sample in the whole sample set $h_f(x)$

the machine learning technique trains the models based on features.

GNSS positioning accuracy is affected by the spatial distribution of satellites, and it is better when the satellites are evenly distributed around the user. In order to make better use of satellite information in the effective space region and reduce the influence of irrelevant GNSS features, the estimation of the positioning error in different space regions should be adjusted, respectively. Considering that the estimation of GNSS positioning error is generally divided into north and east estimated positioning error, the observations were divided into two parts, ultimately creating the north- and east-direction models separately. It should be noted that the division of space region is only for the convenience of positioning accuracy analysis and has nothing to do with the road direction.

According to the azimuth, satellite distributions were divided into four groups (Tan et al. 2019), with the ranges of each shown in Fig. 2. Accordingly, *EL*, C/N_0, and N_{sat} in each group were calculated, respectively, where satellites in *D1* and *D3* were more beneficial for positioning in the north–south direction, and those in *D2* and *D4* were more favorable for positioning in the east–west direction. Satellite data from each of the four groups were used to obtain both the north- and east-direction models.

Principal component analysis (PCA) is often used to reduce the dimensionality of feature classes, preserving those that contribute the most to reducing noise and uncertainty. PCA employs orthogonal transformations to linearly convert a set of potentially correlated observations into uncorrelated variables, known as principal components, the first of which has the maximum variance (nondimensional parameter). Further mathematical details on PCA can be found in Roweis (1997). As GNSS features contain a variety

of information in different aspects, PCA was applied to analyze their priority in classification.

Although there are differences in the feature values for each group, the significance of the features themselves is identical. Hence, the north direction was taken as an example to show the importance of GNSS features based on PCA analysis, as shown in Table 2. The variance ratio of principal components accounted for at least 95% in this study. Among them, PCA-1 had a contribution ratio of 55.7%. Furthermore, Table 2 shows that observation-based features such as *EL*, C/N_0, and N_{sat} were the most indicative parameters, followed by solution-based features. Notably, north dilution of precision (*NDOP*) was calculated using *EL* and azimuth; thus, it yielded little benefit.

Solution-based features, such as the carrier residual (*L1RMS*), Doppler residual (*DopRMS*), and whether the ambiguity is fixed or not (*Ambiguity*), are the indicators of centimeter-level positioning and are of limited value in the proposed method. Additionally, *Position* STD_N is the standard deviation of north GNSS positioning error and mainly refers to the estimated error provided by GNSS positioning solutions, whereas the pseudorange residual (*CARMS*) can better reflect multipath effects. Although these latter two solution-based features matter more than others, their significance is far below that of *EL* and C/N_0; thus, it was concluded that solution-based features account for limited importance during GNSS gross error detection.

The differences between models trained on observation-based features and full features were also tested, with the results showing that the former and latter models had accuracies of 98.5% and 98.6%, respectively. From the negligible differences between the two models, it is obviously concluded that the observation-based features were sufficient enough to accurately model the estimated GNSS positioning error. Therefore, in the following model training, the observation-based features, such as *EL*, C/N_0, and N_{sat} were essential, while those solution-based features were of little account.

Traditional threshold setting method

To more effectively eliminate gross errors and ensure the GNSS positioning accuracy, *EL*, C/N_0, N_{sat}, and *HDOP* are commonly used features in traditional threshold setting methods, beyond which the positioning results are typically considered inaccurate. Typically, reliable positioning can be obtained with N_{sat} greater than 6, whereas the ionospheric and tropospheric delays received by satellites with small elevation angles are relatively large, resulting in greater residual error after correction. Accordingly, the general receivers set a cut-off elevation of 5–15° for removing most multipath-included false alarms. C/N_0 is a basic navigation signal quality parameter capable of characterizing a portion

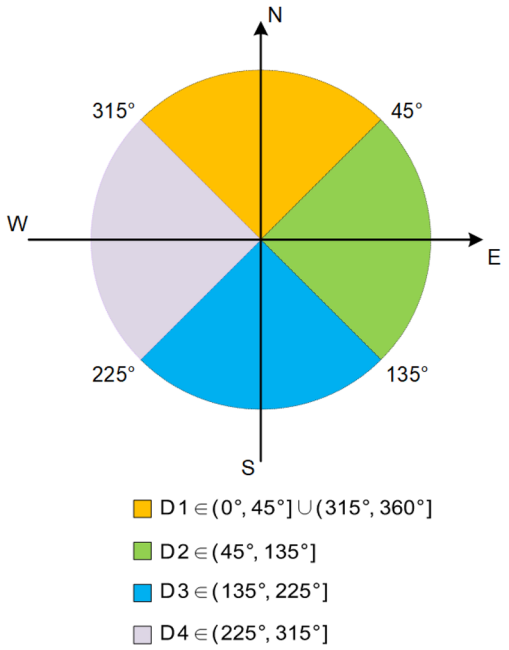

Fig. 2 Satellite group division. *D1*, *D3* belong to the N-S direction; *D2*, *D4* belong to the E-W direction

of the pseudorange observation quality. For satellites with an *EL* of 30°, the typical C/N_0 is 47 ~ 50 dB-Hz, while positioning performance degrades when the C/N_0 of satellites is less than 39 dB-Hz. *HDOP* reflects the distribution of navigation satellites in the sky observable by the receiver, thereby indicating the quality of horizontal positioning from the side (Zhu 1992). Thresholds were set according to:

$$(N_{sat} > T_{N_{sat}}) \wedge (EL > T_{EL}) \wedge (C/N_0 > T_{C/N_0}) \wedge (HDOP < T_{HDOP}) \quad (2)$$

where $T_{N_{sat}}$, T_{EL}, T_{C/N_0}, and T_{HDOP} represent the thresholds of N_{sat}, *EL*, C/N_0, and *HDOP*, respectively. These thresholds are assigned and analyzed in the experimental section.

CART-Bagging-Based Consistency Optimization of GNSS Positioning Error Estimation

The consistency optimization method of GNSS positioning errors based on the CART-Bagging algorithm is described in this section. First, the dataset was partitioned for training, and the performance of the classification model was tested. Subsequently, the obtained class results were used to optimize the estimated error provided by the GNSS solution.

Dataset labeling

As the study aimed to build a classification model for corresponding GNSS positioning error to accuracy classes via

Table 2 GNSS feature significance analyses based on PCA (North-direction model example)

Aspect	Features	PCA-1	PCA-2	PCA-3	PCA-4
Observation	EL_{D3}	0.5899	−0.5145	−0.4148	0.4027
	EL_{D1}	0.5144	0.6333	−0.4327	−0.3814
	$(C/N_0)_{D3}$	0.4866	−0.3759	0.4597	−0.4745
	$(C/N_0)_{D1}$	0.3706	0.4372	0.5464	0.5980
	$(N_{sat})_{D3}$	0.0506	−0.0229	0.1510	−0.2274
	$(N_{sat})_{D1}$	0.0338	0.0277	0.1037	−0.0471
	NDOP	−0.0090	0.0002	−0.0243	0.0158
Solution	*CARMS*	−0.0446	−0.0104	−0.0919	−0.0256
	Position STD_N	−0.0295	−0.0014	−0.0704	0.0399
	Ambiguity	−0.0095	−0.0001	−0.0310	0.0149
	DopRMS	−0.0006	−0.0001	−0.0037	0.0008
	L1RMS	0.0001	0.0000	0.0004	−0.0003
Variance Ratio		55.7%	32.0%	6.6%	2.9%

GNSS features, these accuracy classes were employed as labels. Notably, different GNSS solution modes correspond to different accuracy class division methods, while the division accuracy of the classes also determines the accuracy of the method as well. RTK is a common positioning technique capable of meeting the high-precision navigation and positioning requirements of autonomous driving. Considering the centimeter-level positioning accuracy of RTK, ten GNSS accuracy bands were graded in Table 3, where the error range represents the GNSS north- or east-positioning error compared with the ground truth value. For GNSS solution modes with low positioning accuracy, such as SPP, the step size of the error range could be adjusted to a larger scale.

Here, five-fold cross-validation (Refaeilzadeh et al. 2009) was performed on the dataset to evaluate the performance of classification, where 20% of the data was used for testing and the remaining 80% for training. Figure 3 shows the confusion matrix of north-direction model accuracy, where all blank spaces represent none. Model recognition accuracy reached 100% for positioning with large errors, indicating its usefulness for detecting GNSS gross errors. Alternatively, model accuracy reached more than 96% for positioning with small errors. As the differences in error class grade 1 are relatively small, incorrect detection does not substantially impact GNSS/INS integrated navigation system. Accordingly, the overall model accuracy reached 98.5%, indicating the good classification performance of the algorithm trained on the artificially labeled dataset.

Optimized GNSS error estimation based on classification prediction

Once GNSS positioning has been mapped to an accuracy class grade, the GNSS error estimation should be adjusted for consistency with the actual accuracy. The predicted positioning accuracy class ($\hat{c}$) was obtained through the model. The process of the estimated error optimization is calculated according to:

$$\hat{\sigma} = \sigma * 2^{\hat{c}-c} \tag{3}$$

where σ signifies the north or east estimated error provided by the GNSS solution; c is the class grade provided by the GNSS positioning solution; and $\hat{\sigma}$ is the optimized estimation error capable of forming a more accurate measurement covariance matrix in Kalman filtering, thereby benefitting the GNSS/INS integrated navigation system. Figure 4 gives the flowchart of the CART-Bagging-based GNSS quality control method.

Algorithm performance evaluation indicators

Specific indicators were defined to better evaluate the performance of the CART-Bagging-based GNSS quality control method and its improvement upon the GNSS/INS integrated navigation system. Although the positioning samples in the dataset where the estimated error was inaccurate accounted for a relatively small proportion, the primary purpose of quality control is to improve the positioning accuracy of these epochs. Accordingly, these samples were identified and analyzed separately. The required correction epoch (RCE) was used to evaluate the GNSS quality control method performance, where RCE is defined as the GNSS epoch where the difference between the estimated GNSS error and actual positioning error is more than 2 times, and the actual GNSS positioning error is larger than 1 m. RCE can cause large positioning errors in the integrated navigation system when quality control methods are absent; thus, these epochs were thought to be effectively identified and corrected here. The positioning improvement effect of RCE could be drowned out when analyzing the entire dataset. Therefore, several indicators were proposed:

1) Classification performance aspect.

Model prediction accuracy (η_{Accurate})—Percentage of correct predictions made by the model over the dataset.

Identification ratio of RCE (η_{IR})—A prerequisite for correction, calculated according to:

$$\eta_{IR} = \frac{n_1}{N_{RCE}} * 100\% \tag{4}$$

Table 3 Ten classes of GNSS positioning accuracy

Class grade	Error range (m)	Class grade	Error rang (m)
1	0–0.10	6	1.60–3.20
2	0.10–0.20	7	3.20–6.40
3	0.20–0.40	8	6.40–12.80
4	0.40–0.80	9	12.80–25.60
5	0.80–1.60	10	> 25.60

where N_{RCE} is the total number of RCE in the data, and n_1 is the number of epochs recognized by the proposed model in N_{RCE}.

2) GNSS positioning aspect.

Consistency between the actual GNSS positioning error and the estimated GNSS error (ΔC)—From the perspective of GNSS positioning, the estimated error is expected to match the actual positioning error of GNSS to the maximum extent possible. This consistency is defined according to:

$$\Delta C = \left| \sum_{i=1}^{N} \frac{\sigma_i^2}{N_{\mathrm{all}}} - \sum_{i=1}^{N} \frac{\mathrm{err}_i^2}{N_{\mathrm{all}}} \right| \tag{5}$$

where σ denotes the estimated GNSS error; err represents the actual positioning error of RTK; N_{all} indicates the total number of epochs; and the difference between the statistical value of the estimated error from GNSS processing, and the statistical value of the actual positioning error corresponding to the ground truth was defined as ΔC. When ΔC was close to 0, and the estimated GNSS error is consistent with the actual positioning error.

Consistency improvement ratio (η_{GNSS}):

$$\eta_{\mathrm{GNSS}} = \frac{\left(\Delta C_{\mathrm{original}} - \Delta C_{\mathrm{optimized}}\right)}{\Delta C_{\mathrm{original}}} * 100\% \tag{6}$$

where $\Delta C_{\mathrm{original}}$ denotes the consistency of the original estimated error, $\Delta C_{\mathrm{optimized}}$ represents the optimized consistency of the estimated error, and η_{GNSS} indicates the consistency improvement ratio of the estimated GNSS error.

3) Integrated navigation aspect.

Correction ratio (η_{CR})—The estimated error was corrected after being identified and calculated according to:

$$\eta_{CR} = \frac{n}{N} * 100\% \tag{7}$$

where n is the number of epochs in which integrated navigation results are better (i.e., smaller positioning error) following the estimated GNSS error optimization, and N is the total number of optimized epochs.

The RMS of the positioning error (RMS) in the integrated navigation system compared with the ground truth.

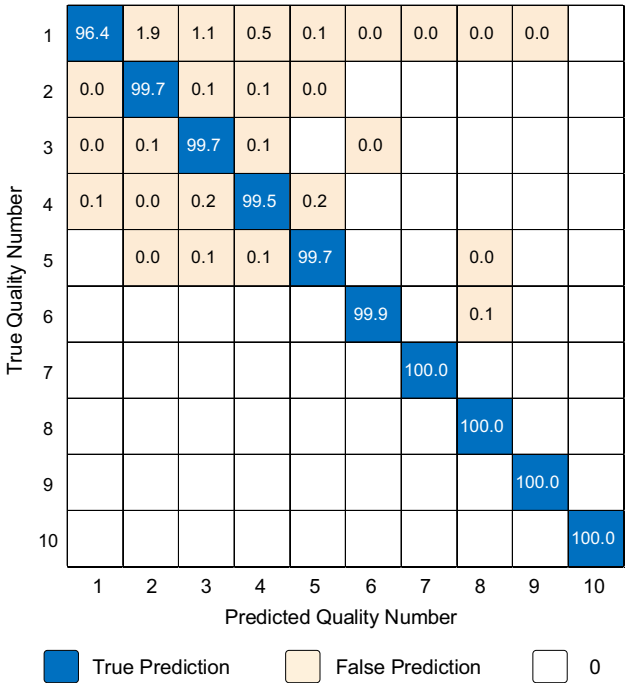

Fig. 3 Confusion matrix for using the CART-Bagging algorithm. The values are in percent

Error reduction ratio (η_{ER})—Measurement of the improvement effect, as calculated with:

$$\eta_{\mathrm{ER}} = \frac{\mathrm{RMS}_{\mathrm{original}} - \mathrm{RMS}_{\mathrm{optimized}}}{\mathrm{RMS}_{\mathrm{original}}} * 100\% \tag{8}$$

where RMS_{original} signifies the RMS of the positioning error in original integrated navigation, and $RMS_{\mathrm{optimized}}$ represents the RMS of the positioning error in optimized integrated navigation.

Experiments and analysis

To make the evaluation results representative and statistically significant, we carried out several field experiments under various conditions to evaluate the CART-Bagging-based performance of the GNSS quality control method. GNSS positioning accuracy and GNSS/INS integrated navigation performance of the full dataset (untrained data included) are presented and discussed in this section.

Experimental description

Figure 5 shows the complete test trajectory in Wuhan; here, a dataset consisting of more than 24 h of GNSS measurements was compiled from typical urban scenes, such as open skies, ring roads, industrial parks, and urban high-rises. At

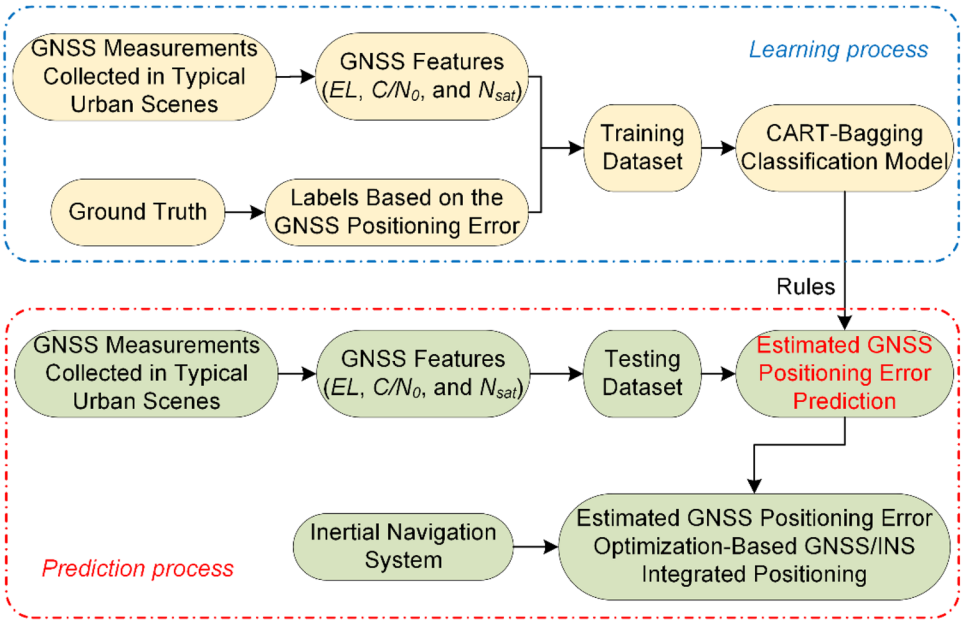

Fig. 4 Quality control process based on the CART-Bagging algorithm. This process includes two steps: classification model using CART-Bagging and consistency optimization of estimated GNSS error based on the model

least three sets of data were collected for each scene, while Table 4 describes the characteristics of each scene in detail. In this dataset, measurements with inconsistent estimated GNSS error accounted for about 25% of all records.

The proposed method is applicable to any conventional receiver. But it should be noted that the model trained by different types of receivers will be different because of their performance variations. Here, a low-cost GNSS/INS integrated navigation system, consisting of a NovAtel 718D GNSS receiver board and a microelectromechanical system (MEMS) inertial measurement unit (IMU) ADIS16460, was used to evaluate the performance of the proposed GNSS quality control method. The post-processed navigation results based on tactical-grade GNSS/INS POS320 were used as the ground truth. The main technical parameters of the two IMUs are listed in Table 5, where the ADIS16460 parameters were optimized by experiment.

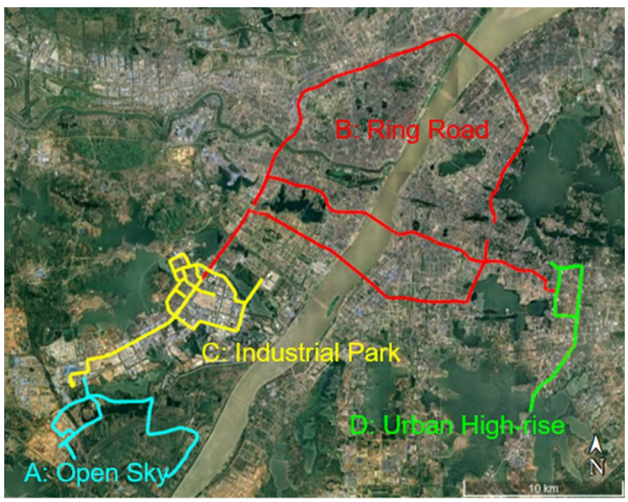

Fig. 5 Test trajectories covering typical urban scenes. Open Sky (blue A), Ring Road (red B), Industrial Park (yellow C), and Urban High-rise (green D)

Results analysis and discussion

To evaluate the CART-Bagging-based GNSS quality control method in different aspects, the efficacy of the classification model, improvement of estimated GNSS positioning error consistency, and the GNSS/INS positioning accuracy were all examined. Both the training (training with test data) and test (training without test data) datasets were assessed to prove feasibility. Moreover, comparative results of the proposed and traditional methods were presented to determine the most optimal approach.

Improvement performance based on training dataset

GNSS features readily vary across analysis periods. To train the classification model covering all characteristics of GNSS in different scenes, training data contained the test data. The results of the training set for four scenes are presented in Tables 6, 7 and 8 to better evaluate the proposed methods from the current study, while Fig. 6 illustrates the original and optimized GNSS error estimation in the east direction of a common case.

Table 6 unanimously displays that η_{Accurate} was 100% for all scenes; thus, all RCEs can be identified. Under this high-accuracy classification model, the optimized GNSS error estimation was more consistent with the actual positioning error, and the η_{GNSS} increased by 95% in the north and 83%

Table 4 Scene descriptions in the experiments corresponding to Fig. 5

	Scenes	Description
A	Open Skies	Less than 10% of GNSS measurements are blocked by buildings and trees, and there are no RCEs during the whole data collection process
B	Ring roads	Tunnels, soundproof sheds/walls, and viaducts are included. Inconsistency of the estimated GNSS error, which results in significant position drift error during GNSS interruption, can occur when driving in and out of these environments, because the valid number of satellites, distribution, and signal quality of satellites are disturbed
C	Industrial Parks	There are small buildings but many trees in this routine. The dense leaves interface GNSS signals and interrupt the positioning results intermittently
D	Urban High-rises	Commercial districts with high-rise buildings account for the majority. Due to severe shadow, only the overhead satellites can be received; and the available satellites yield poor distribution

Table 5 Technical parameters of the IMUs used in the experiments

IMU sensors	Parameters	Low-cost system ADIS16460	Ground truth system POS320
Gyro	Bias ($°/h, 1\sigma$)	12	0.5
	Noise ($°/\sqrt{h}, 1\sigma$)	0.2	0.05
Accel	Bias ($mGal, 1\sigma$)	100	25
	Noise ($m/s/\sqrt{h}, 1\sigma$)	0.2	0.1

in the east statically. For the integrated navigation positioning error, the η_{CR} of optimized epochs and RCEs was more than 75% and 60%, respectively, while the η_{ER} of the positioning error for all optimized epochs and RCEs reached 48% and 42%, respectively. The RMS of the positioning error of RCEs decreased from 4.0 to 2.5 m. Ultimately, the results showed that GNSS positioning error consistency and integrated positioning accuracy were both significantly improved.

Figure 6 compares the estimated error provided by the GNSS solution and the proposed optimization method. The top panel shows that the optimized GNSS estimated error was significantly more consistent with the actual positioning error on the top panel. The bottom panel shows that the integrated navigation results using the optimized GNSS estimated error exhibited a markedly low positioning error on the bottom panel.

Table 6 Classification indicators for the training dataset

Scenes		$\eta_{\text{Accurate}}(\%)$	η_{IR} (%)
A	N	100	/
	E	100	/
B	N	100	100
	E	100	100
C	N	100	100
	E	100	100
D	N	100	100
	E	100	100
Average	N	100	100
	E	100	100

Improvement performance based on test dataset

We tested the model on the untrained dataset to evaluate the improvement effects and universality of the classification model in practical applications. Similarly, the statistical results of the test dataset are listed in Tables 9, 10 and 11, and Fig. 7 displays that the more accurate estimated error ensured the positioning accuracy of the integrated navigation system.

From Tables 9, 10 and 11, it can be observed that the η_{Accurate} of the model for the test dataset was 90%, η_{IR} *was* 80%, and η_{GNSS} was improved by more than 60%. For the optimized epochs and RCEs, η_{CR} and η_{ER} reached 60% and 25%, respectively. Moreover, the RMS of the positioning

Table 7 GNSS positioning error consistency indicators for the training dataset

Scenes		$\Delta C_{\text{original}}$ (m)	$\Delta C_{\text{optimized}}$ (m)	η_{GNSS} (%)
A	N	0.08	0.00	100
	E	0.12	0.00	100
B	N	0.67	0.02	97
	E	0.40	0.02	95
C	N	0.54	0.04	93
	E	1.62	0.39	76
D	N	0.42	0.02	95
	E	0.58	0.05	91
Average	N	0.43	0.02	95
	E	0.68	0.12	83

Table 8 Integrated navigation accuracy indicators for the training dataset

Scenes		All optimized epochs				RCEs			
		$\eta_{CR}(\%)$	$RMS_{\text{original}}(m)$	$RMS_{\text{optimized}}(m)$	$\eta_{ER}(\%)$	$\eta_{CR}(\%)$	$RMS_{\text{original}}(m)$	$RMS_{\text{optimized}}(m)$	$\eta_{ER}(\%)$
A	N	86	1.02	0.49	52	/	/	/	/
	E	83	0.65	0.21	68	/	/	/	/
B	N	77	3.46	2.13	38	71	6.07	3.78	38
	E	77	1.74	0.74	57	73	2.31	1.12	52
C	N	75	1.91	0.86	55	77	3.32	1.56	53
	E	65	2.80	1.83	35	58	4.84	3.52	27
D	N	76	1.12	0.43	62	82	2.60	0.84	68
	E	65	1.65	0.80	52	60	3.83	1.73	55
Average	N	79	2.12	1.19	48	76	4.27	2.41	48
	E	72	1.87	1.07	48	63	3.80	2.35	42

error of RCEs decreased by 1 m. Although these indicators decreased slightly relative to the model for the training dataset, the optimized method can still effectively improve the positioning performance of the system in practice.

Table 11 displays that the performance of the model yielded large differences across the four scenes, with the η_{ER} of the urban high-rise scene being the most significantly improved compared with other scenes. From one perspective, it was revealed that a model trained on a single scene is likely to be superior. The positioning accuracy of the integrated navigation system depends not only on the measurement covariance matrix accuracy but also on the state covariance matrix accuracy. In scenes B and C, even if 60% estimated GNSS error was adjusted correctly for consistency with the actual positioning error to build the high-precision measurement covariance matrix, the improvement effects of integrated navigation position would still not be obvious.

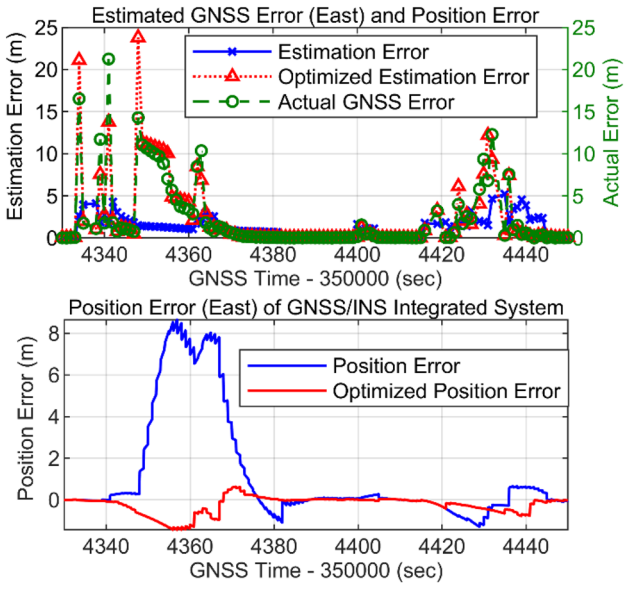

Fig. 6 Estimated GNSS error (east) and position error for the training set (top panel), Comparison of integrated navigation results (bottom panel)

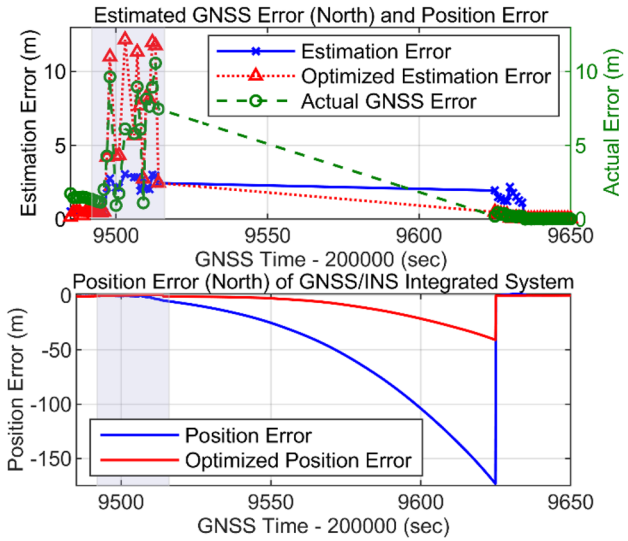

Fig. 7 Estimated GNSS error (north) and position error for the test dataset (top panel), Comparison of the integrated navigation results (bottom panel)

Figure 7 shows a tunnel scene case where the GNSS yielded poor practicability before entering the tunnel between 9495 and 9515 s (gray part). After 9516 s, the experimental vehicle entered the tunnel and exited after about 120 s. For the inertial navigation, the effects of the initial value error on the navigation were manifested significantly over time. The north estimated error provided by the GNSS solution at around 9500 s was mostly lower than the actual positioning error, resulting in large errors of the GNSS/INS integrated navigation results before entering the tunnel. Due to the hysteresis of error imparted by GNSS, the initial position and attitude error forced the inertial navigation results to drift significantly within 120 s in the tunnel. The bottom panel shows that the inertial navigation

Table 9 Classification indicators for the test dataset

Scenes		η_{Accurate} (%)	η_{IR} (%)
A	N	96	/
	E	96	/
B	N	91	86
	E	91	88
C	N	84	91
	E	84	94
D	N	93	94
	E	89	62
Average	N	91	90
	E	90	81

error was significantly reduced after optimizing the GNSS error estimation. This case demonstrated that the proposed method performed well in the tunnel scene, even with the initial unreliable GNSS error estimation.

The proposed method generally performed well in the GNSS/INS integrated system. However, the classification model had one characteristic that strongly correlated with the GNSS features, and the main features of this case in Fig. 8 were inconsistent with the actual positioning error. There was an incorrect classification prediction in the ring road scene, thereby eliminating any statistical improvements imparted by the proposed method as shown in Table 11.

Panel (a) in Fig. 8 shows that at 621 s, the model mistakenly diminished the estimated error of GNSS, thereby increasing the position deviation of the integrated navigation results. In the following seconds, the GNSS quality continued to be poor, and the estimated position of the integrated navigation system diverged more severely. Panels (c-e) revealed that the main features (EL, C/N_0, and N_{sat}) at 621 s did not reflect the abnormality of the GNSS signal and even indicated a better GNSS positioning status. For example, GNSS actual error is less than 5 m at 620 s, while more than 90 m at 621 s. However, EL remained constant and high quality during 620 s and 624 s; C/N_0 maintained a high level above 30 dB-HZ; N_{sat} kept 5. The classification method required that the features correspond to the GNSS error performance. Such abnormal GNSS features, which were beyond the classification ability of the proposed method, seldom occurred, although they resulted in an increased position error was about 5%.

Generally, the proposed GNSS quality control model yielded improved positioning accuracy, demonstrating obvious improvements in terms of GNSS estimated error optimization and integrated navigation results. Specifically, the estimated GNSS positioning error consistency improved by approximately 70%, whereas the GNSS/INS positioning error for all optimized epochs and the RCEs decreased by 25%. Furthermore, the proposed method did not impair the GNSS/INS positioning accuracy when GNSS measurements were of perfect quality. Even if the proposed method incorrectly adjusted the estimated GNSS error, the additional positioning error was less than 10%.

Table 10 GNSS positioning error consistency indicators for the test dataset

Scenes		$\Delta C_{\text{original}}$ (m)	$\Delta C_{\text{optimized}}$ (m)	η_{GNSS} (%)
A	N	0.08	0.03	63
	E	0.12	0.03	75
B	N	0.67	0.05	93
	E	0.40	0.16	60
C	N	0.54	0.05	91
	E	1.62	0.46	72
D	N	0.42	0.25	40
	E	0.58	0.34	41
Average	N	0.43	0.10	78
	E	0.68	0.25	64

Table 11 Integrated navigation accuracy indicators for the test dataset

Scenes		All optimized epochs				RCEs			
		η_{CR}(%)	$RMS_{\text{original}}(m)$	$RMS_{\text{optimized}}(m)$	η_{ER}(%)	η_{CR}(%)	$RMS_{\text{original}}(m)$	$RMS_{\text{optimized}}(m)$	η_{ER}(%)
A	N	74	1.02	0.64	37	/	/	/	/
	E	75	0.67	0.31	54	/	/	/	/
B	N	67	3.51	2.69	23	66	6.34	4.99	21
	E	62	1.63	1.58	3	59	2.32	2.46	-6
C	N	62	1.96	1.67	15	64	3.37	3.12	7
	E	55	2.85	2.56	10	49	4.96	4.25	14
D	N	61	1.12	0.52	54	63	2.68	1.00	63
	E	56	1.69	0.66	61	75	4.40	1.51	66
Average	N	66	1.90	1.38	27	64	4.13	3.04	26
	E	62	1.71	1.28	25	61	3.89	2.74	30

Performance comparison of different quality control methods

Among the numerous methods of GNSS quality control, the traditional threshold setting method is commonly employed for its simple design. To verify the efficacy of the proposed method, the integrated navigation positioning results were compared using the two quality control methods. Referring to the performance of the receiver used in the experiment, $T_{N_{sat}}$, T_{EL}, T_{C/N_0}, and T_{HDOP} were set to 6, 15°, 35 dB-Hz, and 8 in the traditional method, respectively. The optimal thresholds were given in the paper, and if the thresholds changed, the results here were different. Figure 9 shows the cumulative distribution function (CDF) of GNSS/INS positioning error using the traditional threshold setting and proposed CART-Bagging-based GNSS quality control methods.

The GNSS/INS positioning error based on the traditional threshold method yielded limited improvement effects as shown in Fig. 9. For the optimized epochs, 90% and 95% of the position error for the traditional method were within 1.48 m and 2.26 m, respectively, whereas that of the optimized method was within 0.85 m and 0.99 m. The maximum position error of the traditional method (7.03 m) was more than 5 times greater than that of the optimized method (1.39 m); thus, the latter optimization method greatly outperformed the traditional method at diminishing gross position error.

Additionally, it was noted that the traditional method occasionally worsened the positioning results due to the deletion of GNSS epochs with good quality. It was further verified that the CART-Bagging-based quality control model successfully corrected the GNSS error estimation, thereby bringing the optimized GNSS error estimation more consistent with the actual error. Accordingly, it was concluded that the proposed GNSS quality control method outperformed the traditional method of one-size-fits-all.

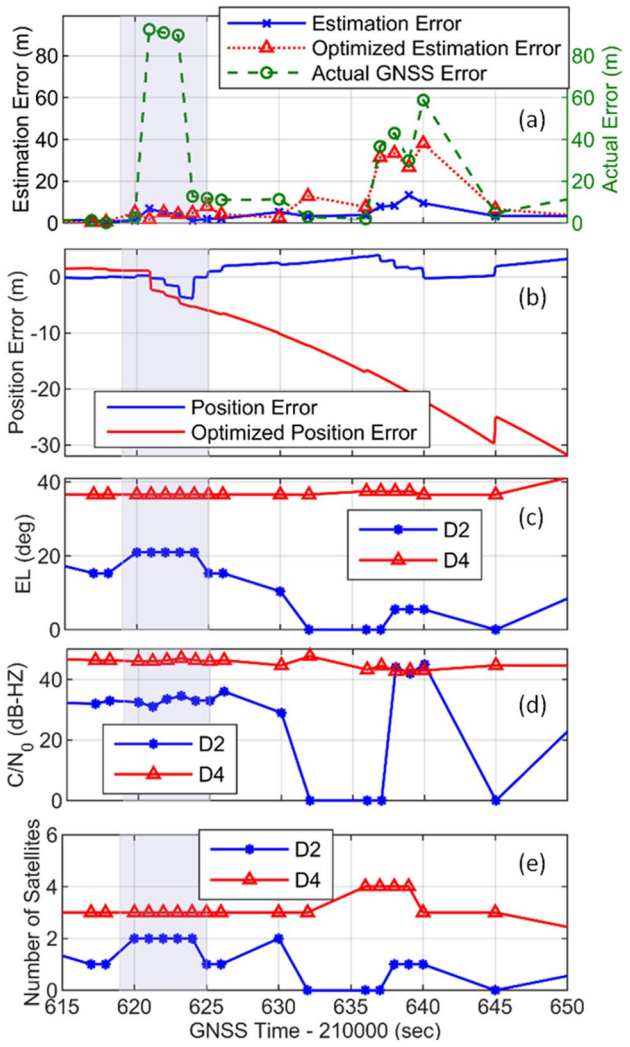

Fig. 8 GNSS position error and the corresponding features. Estimated GNSS error (east) and position error for the bad case (panel a), Comparison of integrated navigation results (panel b), Corresponding principal features: elevation (*EL*), carrier-to-noise density ratio (C/N_0), and number of satellites (N_{sat}) (panel c-e)

Conclusion

The research mainly focuses on improving the consistency of GNSS error estimation to utilize the GNSS measurements more optimally and further improve the positioning performance of the GNSS/INS integrated system. First, a classification model was trained to correspond the GNSS positioning error to ten accuracy classes based on a CART-Bagging algorithm. Only observation-based features, such as *EL*, C/N_0, and N_{sat}, were calculated in each group for the consistency improvement analysis. Then, the classification results were employed to optimize the estimated error provided by

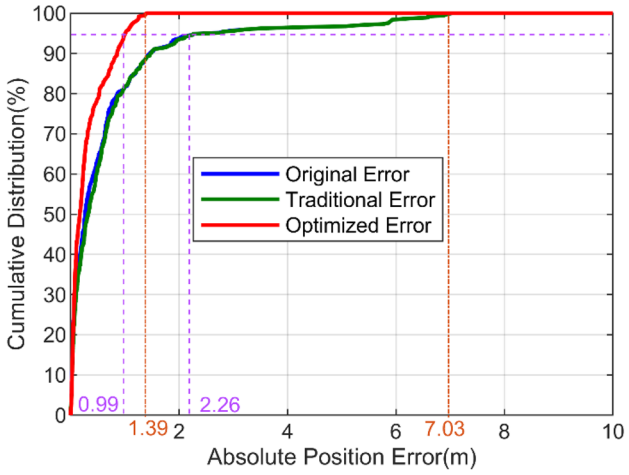

Fig. 9 Comparison of GNSS/INS integrated system position error between the traditional threshold setting and CART-Bagging-based GNSS quality control methods

the GNSS solution. Finally, the optimized GNSS error estimation was applied to guarantee the positioning accuracy of the GNSS/INS integrated system. Multiple field test results of typical urban environments revealed that the model prediction accuracy reached 90%, while the consistency between the estimated GNSS error and the actual positioning error was improved by about 70%, and the integrated navigation positioning accuracy in those estimated GNSS error optimized epochs was improved by approximately 30%. The proposed approach also outperformed the traditional method in the integrated navigation aspect, with 95% of the position error less than 0.99 m, which is only half of the traditional method.

Regarding future directions, the method here only employs observation-based GNSS features, as it is speculated from the bad case study that the current observation features may be unable to cover the entire scene; thus, the introduction of further raw baseband signals of the GNSS receiver could further improve the optimization model for GNSS error estimation. Meanwhile, we will continue to enrich the all-weather and all-scenes datasets to further optimize the accuracy and universality of the model.

Acknowledgements The authors thank Qing Xie and Liqiang Wang for supporting data collection and thank Yan Wang and Jing Fan for their support in the data processing. This work was supported in part by the National Key R&D Program of China (No. 2021YFB2501100, 2022YFB3903802) and the National Natural Science Foundation of China (No. 42174024).

Data availability The raw datasets used in this paper are available by contacting the authors (Xiaoji Niu, xjniu@whu.edu.cn; or Quan Zhang, quanzhang@whu.edu.cn).

References

Breiman L (1996) Bagging predictors. Mach Learn 24(2):123–140
Drawil NM, Amar HM, Basir OA (2012) GPS localization accuracy classification: a context-based approach. IEEE Trans Intell Transp Syst 14(1):262–273
Favenza A, Linty N, Dovis F (2016) Exploiting standardized metadata for GNSS SDR remote processing: a case study. In: Proceedings of ION GNSS + 2016, Institute of Navigation, Portland, Oregon, USA, September 12–16, pp 77–85
Groves PD (2013) Principles of GNSS, inertial, and multisensor integrated navigation systems, 2nd edn. Artech House, Boston
Hsu L-T (2017) GNSS multipath detection using a machine learning approach. In: 2017 IEEE 20th international conference on intelligent transportation systems (ITSC). IEEE, October 16–19, pp 1–6. https://doi.org/10.1109/itsc.2017.8317700
Meng Y, Gao S, Zhong Y, Hu G, Subic A (2016) Covariance matching based adaptive unscented Kalman filter for direct filtering in INS/GNSS integration. Acta Astronaut 120:171–181
Niu X, Wu J, Zhang Q (2018) Research on measurement error model of GNSS/INS integration based on consistency analysis. Gyroscopy Navigation 9(4):243–254
Phan Q-H, Tan S-L, McLoughlin I (2013) GPS multipath mitigation: a nonlinear regression approach. GPS Solut 17(3):371–380
Quinlan JR (1986) Induction of decision trees. Mach Learn 1(1):81–106
Rao CR, Wegman EJ, Solka JL (2005) Data mining and data visualization, 1st edn. Elsevier, San Diego, CA
Refaeilzadeh P, Tang L, Liu H (2009) Cross-validation. Encyclopedia of database systems, 5th edn. Springer, Berlin Heidelberg, pp 532–538
Roweis S (1997) EM algorithms for PCA and SPCA. Advances in neural information processing systems. MIT Press, Cambridge, pp 626–632
Shin E-H (2005) Estimation techniques for low-cost inertial navigation. University of Calgary, Canada. Doctoral dissertation, Department of Geomatics Engineering, Calgary
Socharoentum M, Karimi HA (2016) A machine learning approach to detect non-line of sight satellites in Nav2Nav. Presented at the 23rd ITS World Congress, Melbourne, Australia, October, 10–14
Sun R, Wang G, Cheng Q, Fu L, Chiang K, Hsu L, Ochieng WY (2021) Improving GPS code phase positioning accuracy in urban environments using machine learning. IEEE Internet Things J 8:7065–7078. https://doi.org/10.1109/JIOT.2020.3037074
Sutton CD (2005) Classification and regression trees, bagging, and boosting. Handbook Statist 24:303–329
Takasu T, Yasuda A (2009) Development of the low-cost RTK-GPS receiver with an open source program package RTKLIB. The international symposium on GPS/GNSS. 2009, November 4–6. Jeju, Korea
Tan J, Wang J, Lu D (2019) GNSS data driven clustering method for railway environment scenarios classification. In: Proceedings of 14th IEEE conference on industrial electronics and applications (ICIEA), pp 2026–2031. https://doi.org/10.1109/iciea.2019.8833839
Tangirala S (2020) Evaluating the impact of GINI index and information gain on classification using decision tree classifier algorithm. Int J Adv Comput Sci Appl 11(2):612–619
Xu H, Hsu L-T, Lu D, Cai B (2020) Sky visibility estimation based on GNSS satellite visibility: an approach of GNSS-based context awareness. GPS Solut 24(2):1–15
Zhou R, Hu Z, Zhao Q, Li P, Wang W, He C, Cai C, Pan Z (2018) Elevation-dependent pseudorange variation characteristics analysis for the new-generation BeiDou satellite navigation system. GPS Solut 22(3):60. https://doi.org/10.1007/s10291-018-0726-x
Zhu J (1992) Calculation of geometric dilution of precision. IEEE Trans Aeros Electron Syst 28(3):893–895

Xiaoji Niu received a B.E. degree (with honors) in mechanical and electrical engineering and a Ph.D. degree from Tsinghua University, Beijing, China, in 1997 and 2002, respectively. From 2003 to 2007, he was a Post-Doctoral Fellow with the Mobile Multi-Sensor Systems (MMSS) Research Group, Department of Geomatics Engineering, University of Calgary. From 2007 to 2009, he was a Senior Scientist with SiRF Technology Inc. He is currently a Professor at GNSS Research Center, Wuhan University. His research interests focus on INS and the GNSS/INS integrated system.

Yuhang Dai received a B.E. degree (with honor) in Navigation Engineering from Wuhan University, Wuhan, China, in 2020 and is now pursuing a master's degree in Navigation, Guidance, and Control at GNSS Research Center, Wuhan University. Her main research interests include the GNSS/INS integrated system and visual-based navigation for land vehicles.

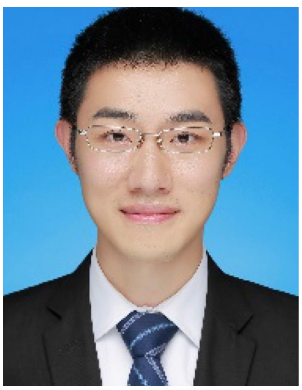

Tianyi Liu received a B.S. degree in electronic information engineering from Wuhan University, Wuhan, Hubei, in 2015 and an M.S. degree in signal and information processing from the Chinese Academy of Science, Beijing, in 2018. He is currently pursuing a Ph.D. degree in communication and information systems at Wuhan University, Wuhan, Hubei, China. His research interests include LiDAR SLAM, integrated navigation, and deep learning.

Qijin Chen received a B.Eng. degree and a Ph.D. degree in Geodesy and Survey Engineering from Wuhan University, Wuhan, China, in 2011 and 2016, respectively. He is currently an Associate Research Fellow with the GNSS Research Center, Wuhan University, Wuhan, China. His research interests focus on INS with aiding and its applications in geodesy and precise surveying engineering, including railway track geometry measuring and undergroundpipeline surveying.

Quan Zhang received a B.S. degree in Geomatics Engineering from Shandong University of Science and Technology in 2009, and a Ph.D. degree from Wuhan University in 2015. From 2017 to 2018, he was a Post-Doctoral Researcher with the Digital Photogrammetry Research Group (DPRG), Lyles School of Civil Engineering of Purdue University. He is currently an Associate Professor of the GNSS Research Center at Wuhan University. His research interests include inertial navigation and GNSS/INS integrated technology for land vehicles.